In-situ Observation of Phase Transition of Silico-Ferrite of Calcium and Aluminum

H.Kim[1], *J.Park* [2] *and J.Lee*[3*]

1. Master Student, Korea University, Seoul 02841. Email: gkdmsskfk789@korea.ac.kr
2. Researcher, POSCO, Gwangyang 57807. Email: J_park@posco.com
3. Professor, Korea University, Seoul 02841. Email: joonholee@korea.ac.kr

Keywords: CLSM, DSC, Iron ore sinter, Phase transition, SFCA

ABSTRACT

Silico-ferrite of calcium and aluminum (SFCA) is a bonding phase in the iron ore sinter. The phase transition upon melting of SFCA was investigated with Differential Scanning Calorimetry and Confocal Laser Scanning Microscope. The initial melting of SFCA occurred at 1183.2ºC, and a massive melting was found at around 1351.1-1358.2ºC. A phase transition-melting was investigated at 1476.5-1478.7ºC. The liquid phase was composed of immiscible phases. The present results would be utilized to design a new iron ore sinter for better processing performance in a hydrogen-enriched ironmaking process.

INTRODUCTION

Iron ore sinter is a feeding material used in the blast furnace(BF) ironmaking process. Iron ore sinter is made of iron ore fines, flux, and coal. Ignition of the coal by oxygen increases the temperature to 1300ºC, resulting in liquid phase sintering of the iron ore particles. A complex mosaic structure is typically found in the iron ore sinter as shown in FIG 1, where the silico-ferrite of calcium and aluminum (SFCA) is the bonding material. Since the reduction of the iron ore sinter in BF starts from the reduction of hematite, SFCA would make the first liquid slag. When hydrogen is introduced in BF to reduce CO_2 emission, the role of SFCA becomes more critical in forming a liquid slag phase [Park 2023, Dereje 2018].

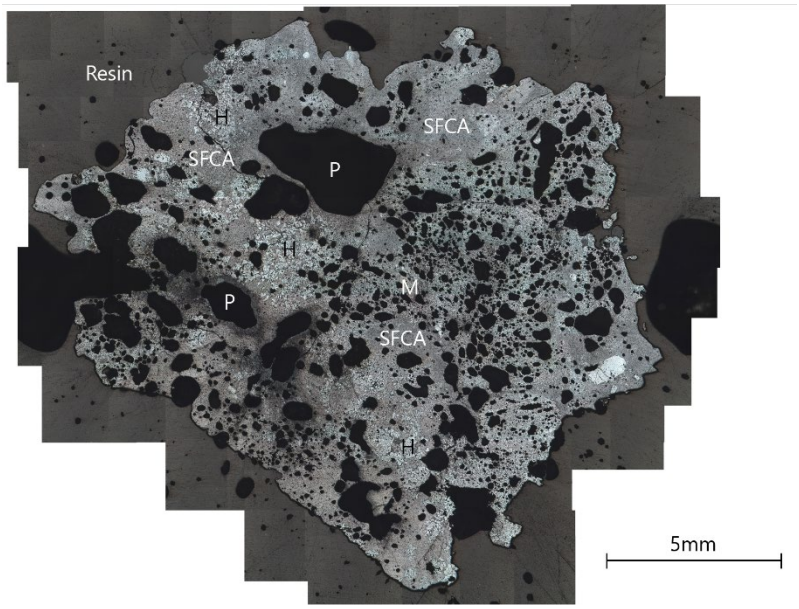

FIG 1 – Commercial iron ore sinter (H:Hematite, M:Magnetite, P:Pore, SFCA)

FIG 2 shows a schematic of the crystal structure of SFCA in the polyhedral model. SFCA (ICDD: 01-080-0850) comprises 14 metal atoms and 20 oxygen atoms, with each metal atom occupying either an octahedral or tetrahedral site and forming bonds with oxygen atoms [Hamilton 1989]. The triclinic space group characterizes the structure of SFCA [Hamilton 1989]. FIG 2 provides a schematic representation of the crystal structure of SFCA, featuring alternating stacking of spinel planes and pyroxene planes [Park 2022]. The unit cell of SFCA possesses lattice parameters a = 9.061Å, b = 10.020Å, and c = 10.920Å [Hamilton 1989]. In specific sites, Ca2+, Fe2+, and Mg2+ are located in the octahedral sites (M1, M2, M3, M7, M10, and M11), while Si4+, Fe3+, and Al3+ occupy the tetrahedral sites (M4, M5, M6, M8, M9, and M12) [Hamilton 1989]. The tetrahedral sites exhibit distinct categorizations: (1) Fe and Al substitution at the M6 site, (2) Si and Al substitution at the M12 site, and (3) Ca and Fe substitution at the Ca1 site. Takayama et al. [Takayama 2018] identified the Mg substitution site based on Hamilton's crystal structure. SFCA has been studied extensively by

many researchers. However, most of them focused on the microstructure of the iron ore sinter and the corresponding crystalline structures.

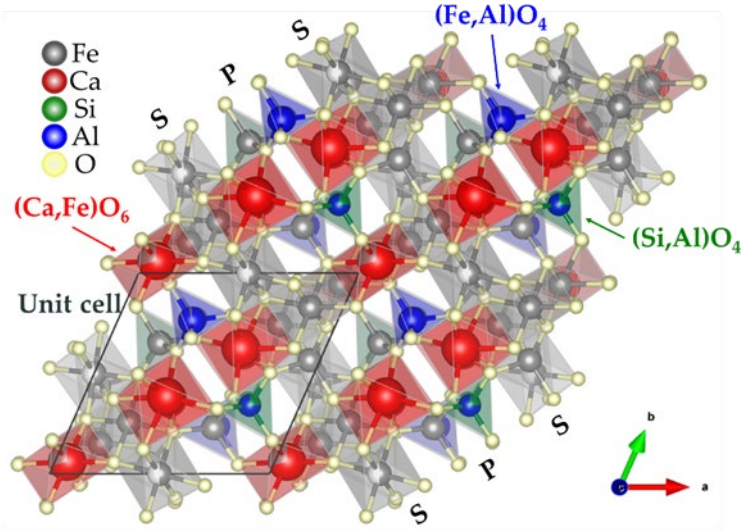

FIG 2 – Schematic of the crystal structure of SFCA in the polyhedral model(with the ball and stick model) indicating the atom substitution position of the tetrahedral ((Si, Al)O4, (Fe, Al)O4) sites and octahedral ((Ca, Fe)O6) sites, and the sequence of spinel (S) and pyroxene (P). [Park 2022]

For the effective utilization of the iron ore sinter in BF, it is essential to understand the phase transitions, especially liquid phase formation. In this study, the phase transition of SFCA with liquid phase formation is investigated using both differential scanning calorimetry (DSC) and confocal laser scanning microscope (CLSM). This new technique is helpful for understanding the liquid phase formation in BF to stabilize the operation condition by achieving a high gas permeability through the coke bed.

EXPERIMENTAL

Sample preparation

Reagent grade chemicals (Fe_2O_3, $CaCO_3$, SiO_2, Al_2O_3, 99.99% purity, <100 μm) were used. $CaCO_3$ was calcinated to obtain CaO at 1273 K for 2 hours in advance. Calcinated CaO was crushed, and particles under 100 μm were collected for sample preparation. The composition of the samples used in the experiment is shown in TABLE 1. Fig 3 shows a schematic illustration of the experimental apparatus. A $MoSi_2$ electric resistance furnace of a maximum temperature of 1600°C was used. A mixture of chemicals with a pre-determined ratio is placed in a platinum-10% rhodium crucible and kept at 1420°C for 12 h to form a liquid phase under a 300 mL/min air gas (21%O_2-79%N_2). The sample is then quenched in a distilled water.

For the successive DSC analysis, synthesized SFCA were crushed under 100 μm using mortar and pestle. For the in-situ observation with CLSM, the bulk SFCA was shaped into a cylindrical sample about 3-4mm in diameter and 1mm in height.

TABLE 1 – The composition of SFCA used in the present experiments.

Composition (mole conc, %)			
Fe_2O_3	CaO	SiO_2	Al_2O_3
48.77	28.74	4.99	17.50

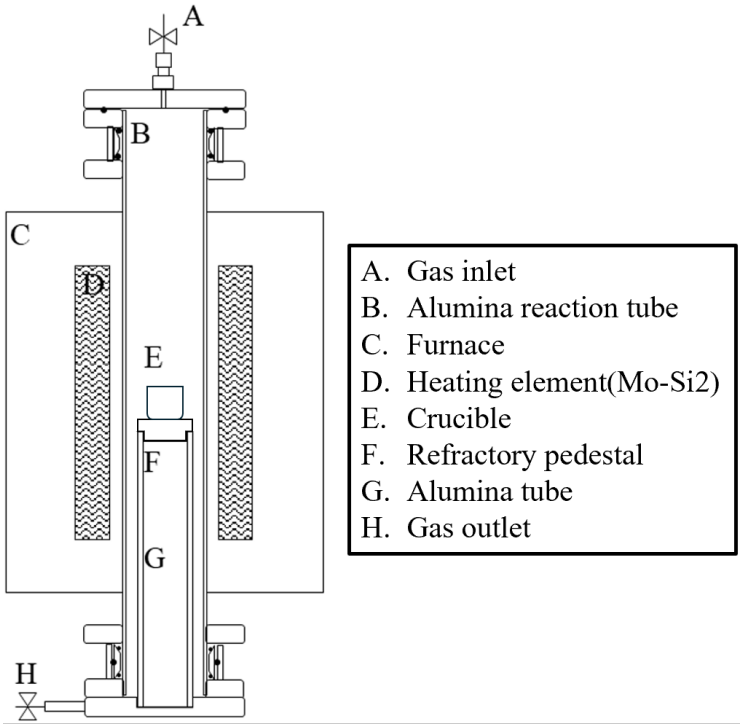

FIG 3 - Schematic diagram of the experimental setup

Phase transition analysis using DSC

DSC analyses were carried out in a simultaneous thermal analyzer STA 449 F5 Jupiter (Netzsch, Germany), as shown in FIG 4. The temperature was calibrated with Benzoic Acid, $BaCO_3$, Ag_2SO_4, and CsCl, all supplied by Netzsch-Gerätebau GmbH. A sample was heated in a platinum-10% rhodium crucible covered with an Al_2O_3 crucible at a heating rate of 50°C/min up to 1000 °C. The sample was then heated at different heating rates (5, 10, 20, 25 °C/min) up to 1500 °C under a purified Ar gas (99.9999% purity) flowing at 50 mL/min.

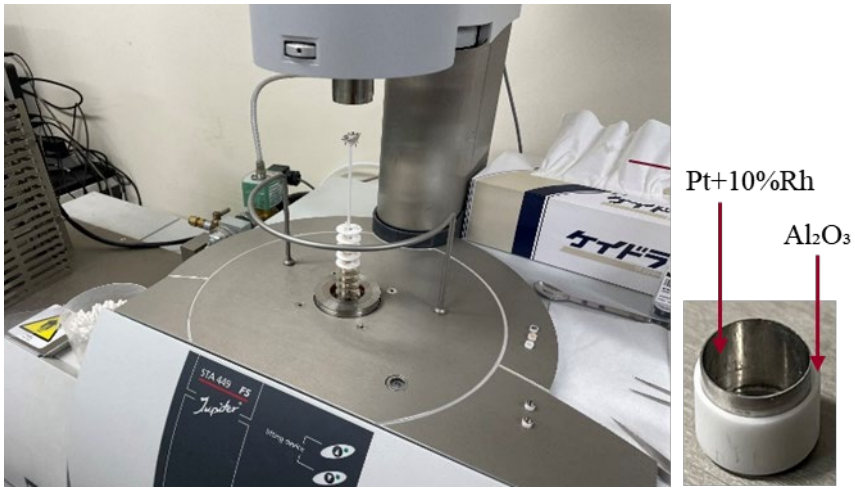

FIG 4 – (L) Differential Scanning Calorimetry equipment(STA 449 F5 Jupiter, Netzsch, Germany) (R) the crucibles used for DSC analysis.

In-situ observation of the phase transition using CLSM

Phase transition of the SFCA was visually observed with CLSM (SVFSP; Yonekura MFG. Co. LTD, Japan), as shown in FiG 5. The observation temperature was calibrated with Au and Ni. The sample temperature increased at 500°C/min up to 1000°C and held at this temperature for 60 s, and then it was heated at 10 °C/min up to 1600 °C, under a purified Ar gas(99.9999% purity) at a flow of 200 mL/min. After experiments, the samples were analyzed with SEM(SU5000, HITACHI, Japan) and EDS(AZteclive Ultim Max40, Oxford, UK). As an exception, FIG 16 and 17 were analyzed with SEM(FEI Quanta FEG 250, Philips, USA) – EDX(Apollo 10, Ametek, USA).

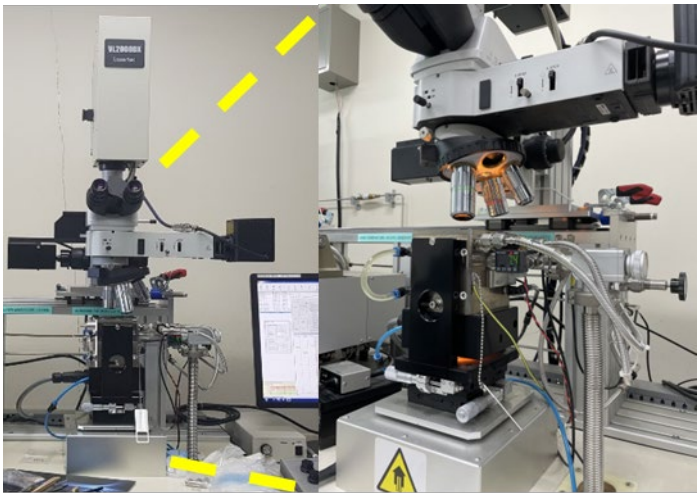

FIG 5 – CLSM equipment(SVFSP; Yonekura MFG. Co. LTD, Japan)

RESULTS AND DISCUSSIONS

Synthesized SFCA

The synthesized SFCA sample was investigated with SEM-EDS. The quenched sample was composed of a Fe-rich SFCA phase and a Ca-Si-Al-rich phase, as shown in FIG 6 and 7. Webster et al.(2021, 2022) characterized the phase transition of the SFCA by using the synchrotron XRD during heating and cooling cycles [Webster 2021, 2022]. Webster et al.(2012) reported that once SFCA is molten to form a liquid phase and Fe_3O_4, Fe-rich SFCA and SFCA are generated successively. TABLE 2 shows the EDS mapping and point analysis results of the synthesized SFCA. EDS mapping confirmed that the overall composition was similar to the target composition in TABLE 1. In addition, EDS point analysis confirmed that the bright area was the Fe-rich area with high Fe components and low Si and Al components, and the dark part was SFCA. Accordingly, the present observation results show a good agreement with those of Webster et al.(2022).

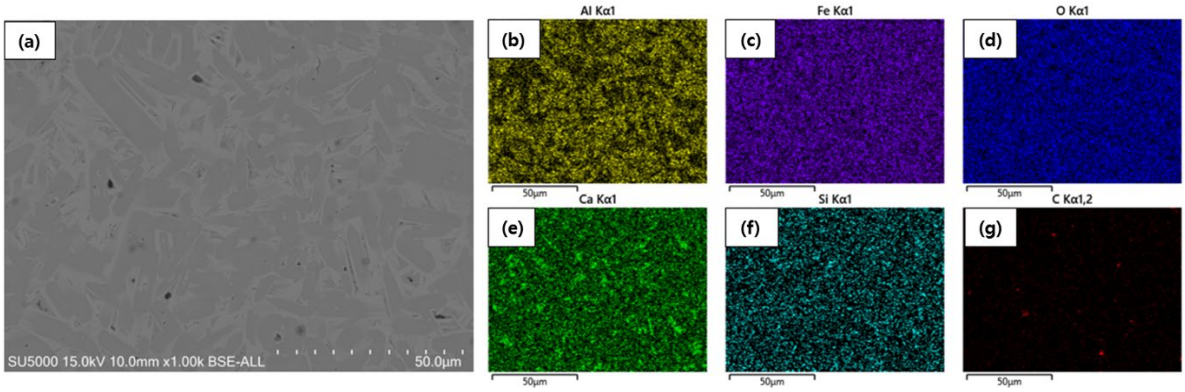

FIG 6 – Results of SEM-EDS analysis of synthesized SFCA (a) BSE micrograph of synthesized SFCA (b) Al signals of EDS of (a), (c) Fe signals of EDS of (a), (d) O signals of EDS of (a), (e) Pt signals of EDS of (a), (f) Ca signals of EDS of (a), (g) Si signals of EDS of (a), (h) C signals of EDS of (a).

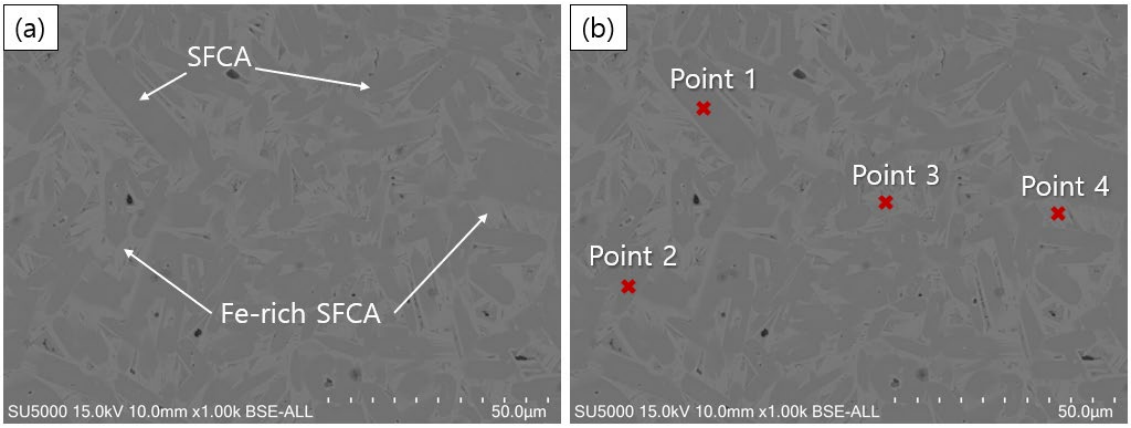

FIG 7 – Microstructure of synthesized SFCA (a) identification of SFCA (dark) and Fe-rich SFCA (bright), (b) analyzed points of synthesized SFCA.

TABLE 2 – EDS results of mapping/point analysis of synthesized SFCA in FIG 7.

	Elemental Compositions (Atomic Conc, %)							Calculated Compotisions (Mole Conc, %)			
	Fe	Ca	Si	Al	O	C	Pt	Fe_2O_3	CaO	SiO_2	Al_2O_3
Mapping	24.55	7.21	1.33	9.29	49.88	7.29	0.49	48.27	28.35	5.11	18.27
Point 1	22.16	6.36	1.46	12.38	50.07	7.12	0.45	44.16	25.35	5.82	24.67
Point 2	22.22	6.34	1.4	12.24	49.58	7.53	0.23	44.49	25.39	5.61	24.51
Point 3	25.76	6.49	1.06	9.32	50.05	6.85	0.48	51.34	25.87	4.22	18.57
Point 4	30.47	6.34	0.59	5.13	48.84	8.12	0.52	61.61	25.64	2.39	10.37

Phase transition analysis results using DSC

FIG 8 shows the DSC curves obtained in the present study. The heating rate was set to 5, 10, 20, and 25 °C /min, respectively. TABLE 3 summarizes the onset point of the first peak, the peak points and the end points of the second and third peaks. The regression of the data points yields data at 0°C /min for the onset, peak2, end2, peak3, and end3 to be 1183.2, 1351.4, 1358.2, 1476.5, and 1478.7°C, respectively. Consequently, it is concluded that SFCA begins to melt at around 1183.2°C, and massive melting occurs through 1351.1-1358.2℃, and complete melting was found at 1476.5-1478.7℃, respectively.

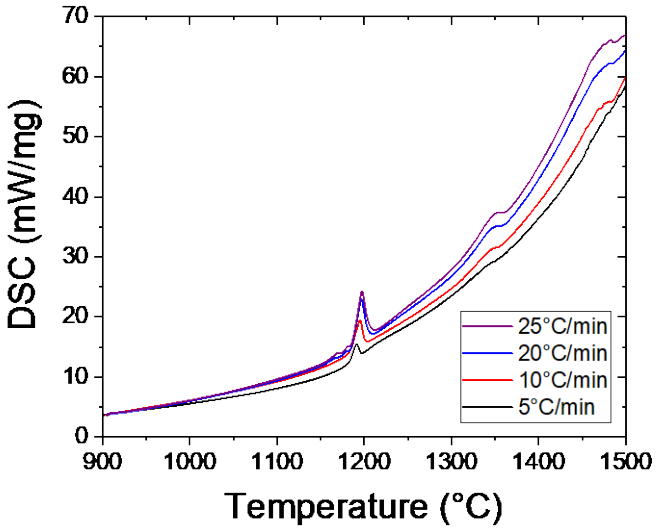

FIG 8 – DSC analysis results by heating rate.

TABLE 3 – DSC analysis results at different heating rates.

	Heating Rate (℃/min)			
Peaks	5	10	20	25
Onset	1183.9	1184.7	1186.0	1186.8
Peak 2	1352.8	1351.9	1353.9	1355.1
End 2	1359.5	1360.0	1363.0	1363.6
Peak 3	-	1479.4	1478.3	1483.4
End 3	-	1483.2	1487.5	1489.9

In-situ observation of the phase transition using CLSM

SFCA of this composition had several notable changes during the melting process. It was analyzed by dividing it into four stages: initial surface modification, initial melting, massive liquid phase formation, and phase transition-melting.

Step 1: Initial surface modification

The initial surface modification observation results are shown in FIG 9. The scratch on the polished SFCA surface was modified due to thermal etching, and the grain boundary of the SFCA was revealed.

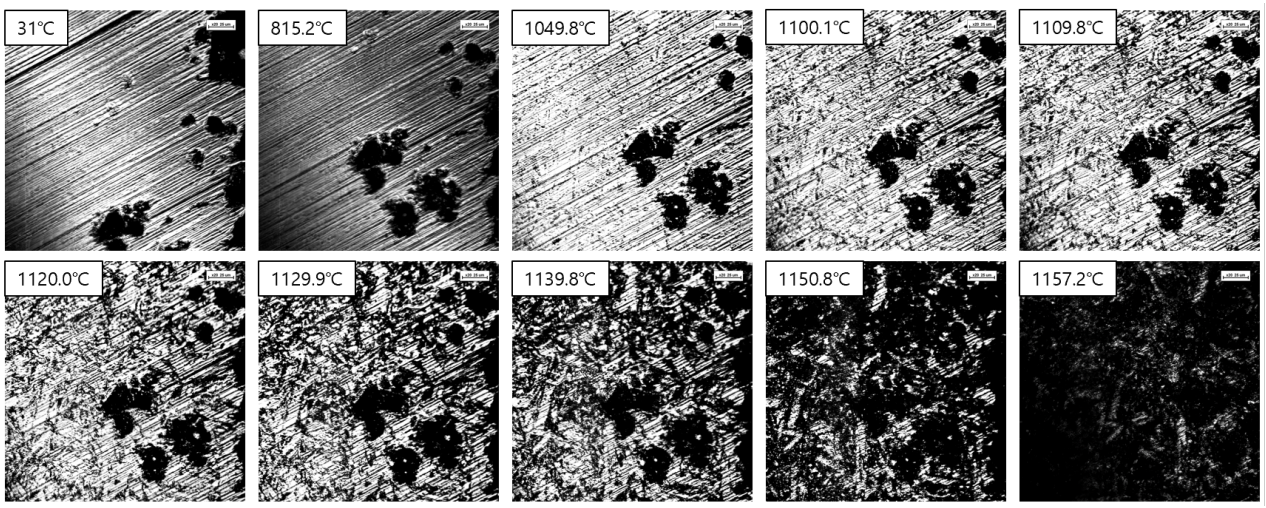

FIG 9 – In-situ observation of initial surface modification using CLSM.

After observing the surface change up to the temperature before the first peak of the DSC result, the sample was rapidly cooled to analyze the surface SEM-EDS. This sample was quenched at 1157.2°C, for a successive EDS mapping. The results of the analysis are shown in FIG 10. Notably, a Ca-Si-Al-rich region is found near the pores. Eventually, this area was found to be the initial melting position from the successive analysis.

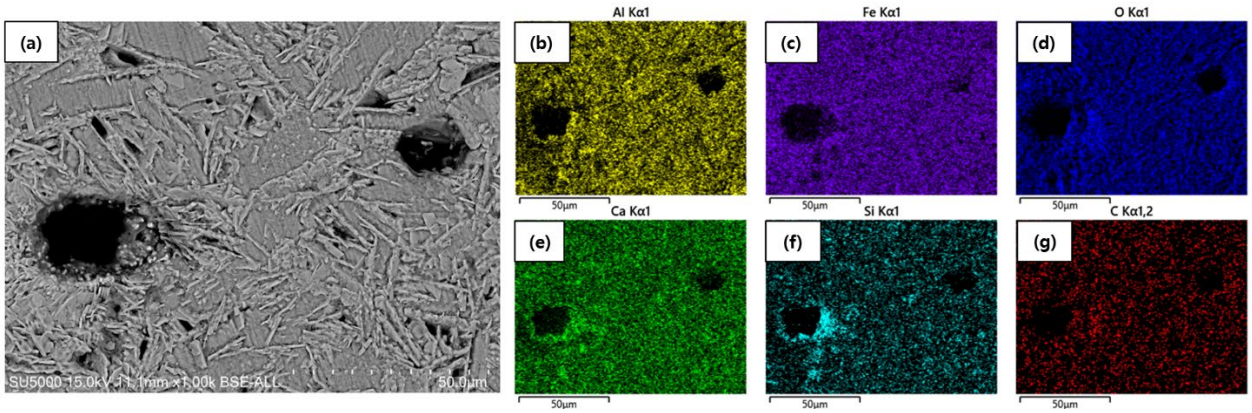

FIG 10 – Results of SEM-EDS analysis of the specimen after the observation of initial surface modification near pore side (a) BSE micrograph of the specimen after the observation of initial surface modification (b) Al signals of EDS of (a), (c) Fe signals of EDS of (a), (d) O signals of EDS of (a), (e) Pt signals of EDS of (a), (f) Ca signals of EDS of (a), (g) Si signals of EDS of (a), (h) C signals of EDS of (a).

Step 2: Initial melting

The observations of initial melting with CLSM are shown in FIG 11. The initial surface melting was observed at around 1196 °C, slightly higher than the point (1183.2 °C) investigated with DSC. Nevertheless, this difference of 12.8 °C is acceptable when we consider a typical error in temperature measurements with CLSM. The sample quenched at 1278.6°C was analyzed with SEM-EDS, shown in FIG 12. It is found that Ca, Si, and Al were segregated on several points, which were indicated with a dark grey color in the SEM image. As shown in TABLE 4, EDS point analysis verified that the initial melting phase was a Ca-Si-Al-rich phase, whereas the matrix was a Fe-rich phase.

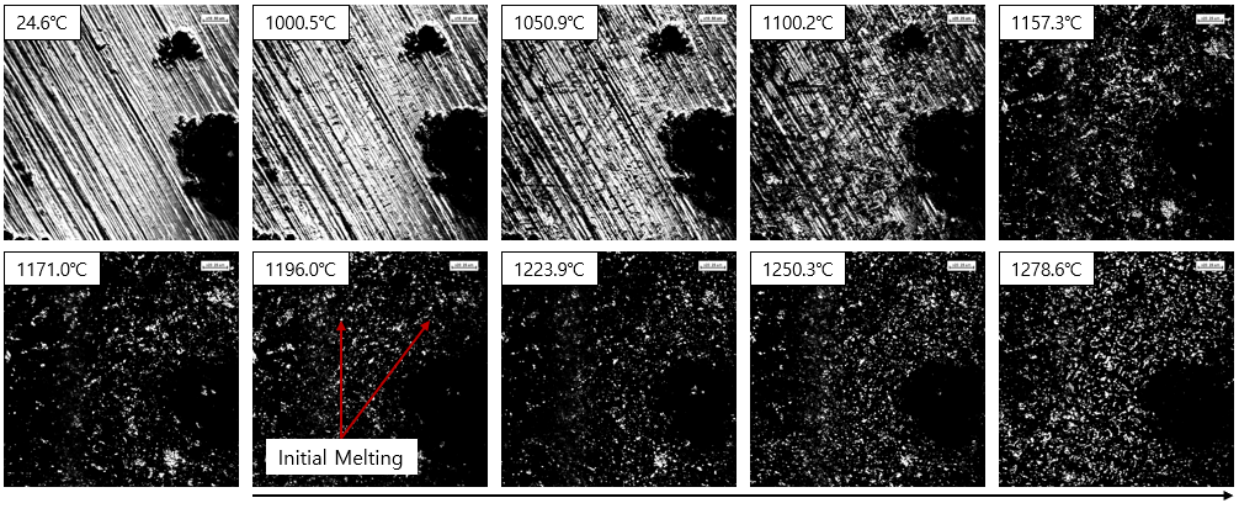

FIG 11 – In-situ observation of initial melting using CLSM.

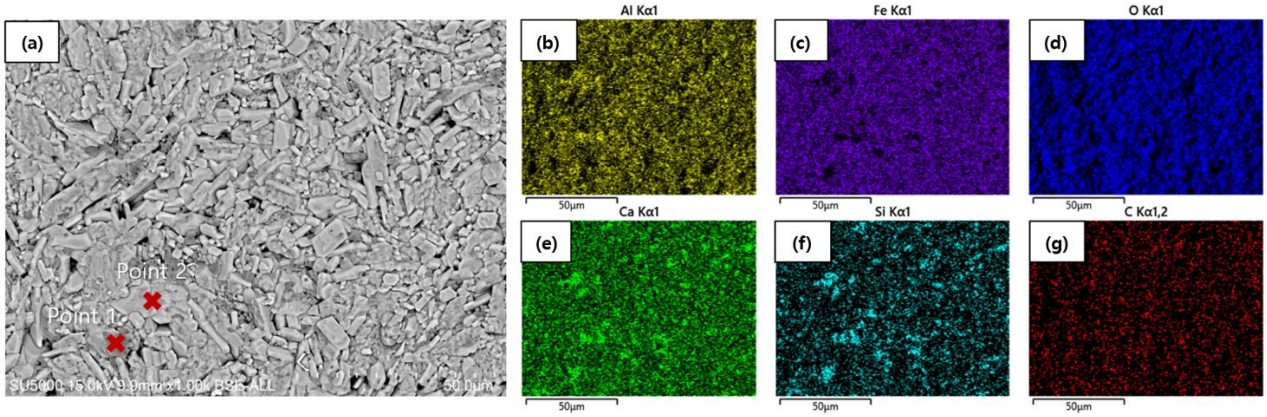

FIG 12 – Results of SEM-EDS analysis of the specimen after the observation of initial surface modification. Dark grey color regions correspond to the initial melting points.

TABLE 4 – EDS results of mapping/point analysis of the specimen after the observation of initial melting shown in FIG 12.

	Elemental Compositions (Atomic Conc, %)							Calculated Compositions (Mole Conc, %)			
	Fe	Ca	Si	Al	O	C	Pt	Fe_2O_3	CaO	SiO_2	Al_2O_3
Mapping	24.68	7.54	1.61	9.09	48.84	7.5	0.73	47.4	28.96	6.18	17.46
Point 1	12.96	19.63	6.79	11.43	42.85	5.5	0.84	16.78	50.84	17.58	14.8
Point 2	30.23	6.35	0.65	8.14	47.36	6.53	0.75	57.72	24.25	2.48	15.54

Step 3: Massive liquid phase formation

DSC results showed a massive phase transition occurs at around 1351.1-1358.2 ºC. Further investigation with CLSM was carried out by 1362.4 ºC, as shown in FIG 13. It was found that a massive liquid phase formation occurred at 1351.6 ºC, which shows reasonable agreement with the DSC data. A liquid phase between small solid islands covered a wide range of the sample. The sample was quenched at 1362.4ºC, and SEM-EDS analysis was carried out successively. As shown in FIG 14 and TABLE 5, the light grey region is CF and CFA, while the dark grey region is indicated to be the liquid Ca-Si-Al-rich phase.

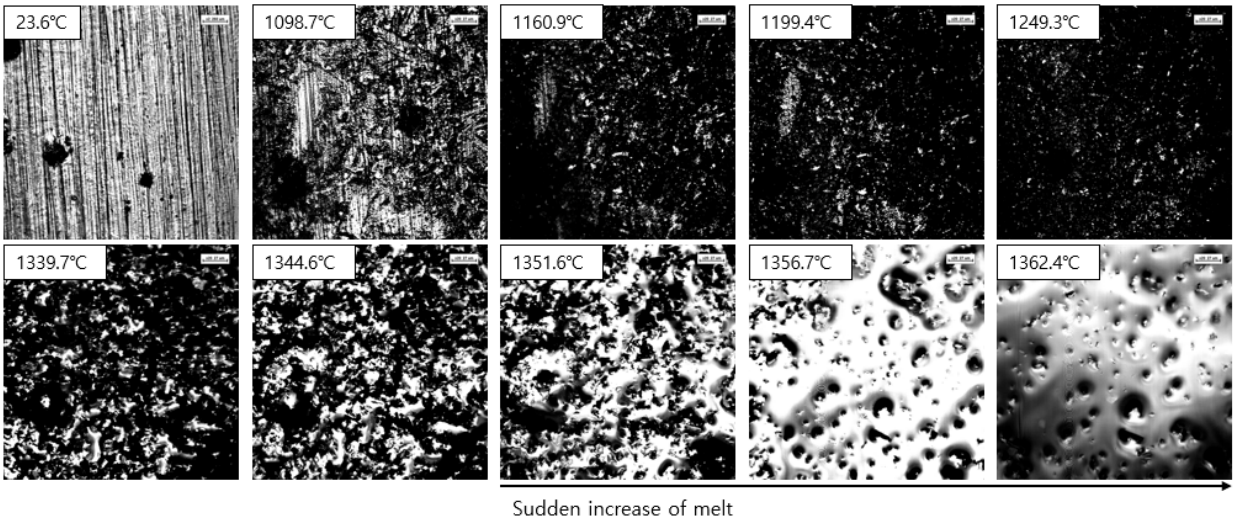

FIG 13 – In-situ observation of an increase of liquid phase using CLSM

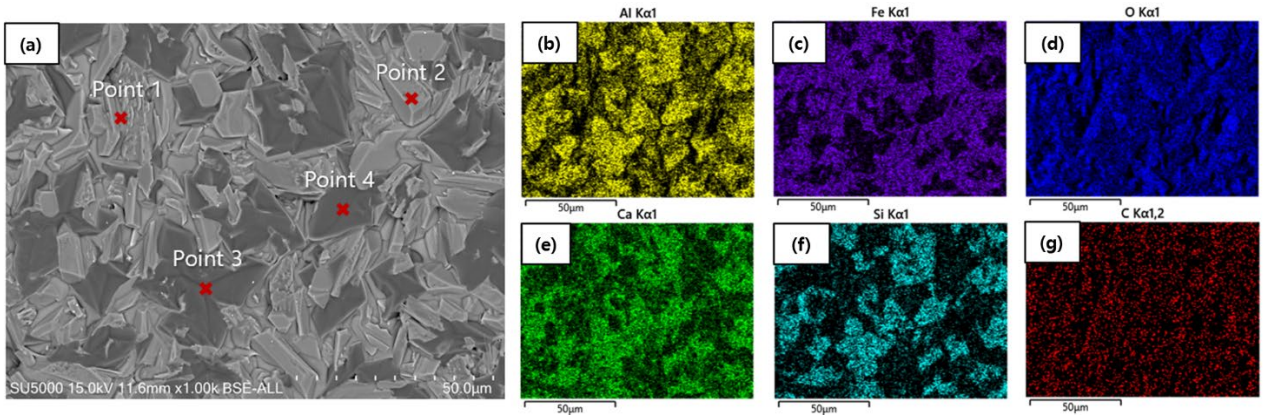

FIG 14 – Results of SEM-EDS analysis of an increase of the liquid phase.

TABLE 5 – EDS results of mapping/point analysis of FIG 14.

	Elemental Compositions (Atomic Conc, %)							Calculated Compositions (Mole Conc, %)			
	Fe	Ca	Si	Al	O	C	Pt	Fe_2O_3	CaO	SiO_2	Al_2O_3
Mapping	18.18	10.89	3.32	10.22	49.46	7.28	0.65	32	38.33	11.69	17.99
Point 1	52.46	22.29	0.49	2.82	17.09	3.68	1.17	52.02	44.21	0.97	2.8
Point 2	24.75	3.82	0.64	9.21	52.81	8.18	0.59	57.72	17.82	2.99	21.48
Point 3	3.3	14.63	7.06	13.92	53.18	7.48	0.44	5.45	48.28	23.3	22.97
Point 4	5.34	15.16	7.01	13.73	50.55	7.77	0.45	8.42	47.82	22.11	21.65

Step 4: Phase transition-melting

DSC results revealed that the last phase transition occurred at 1476.5~1478.7ºC. The CLSM observation shown in FIG 15 supported the fact that the transition was related to the phase transition and successive melting. The cross-section of the quenched sample was investigated with SEM-EDX. The EDX results in FIG 16 show elemental segregation. There were two immiscible phases: the Fe-Al-rich phase and the Ca-Si-Al-rich phase. The Fe-Al-rich phase is considered a Fe_3O_4 solid solution, and the Ca-Si-Al-rich phase is liquid. Webster et al.(2012) reported a similar result that Fe_3O_4 could appear in SFCA at high temperatures.[Webster 2012] Accordingly, it is considered that CF and CFA transformed to Fe_3O_4 solid solution and some amount of CaO and Al_2O_3 dissolved in liquid slag.

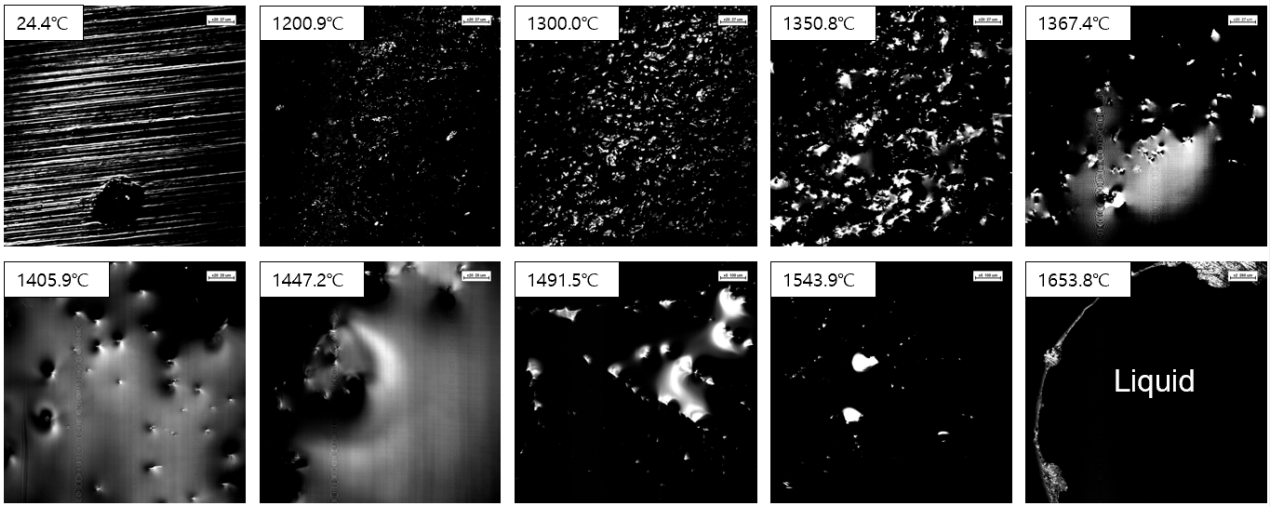

FIG 15 – In-situ observation of complete melting using CLSM

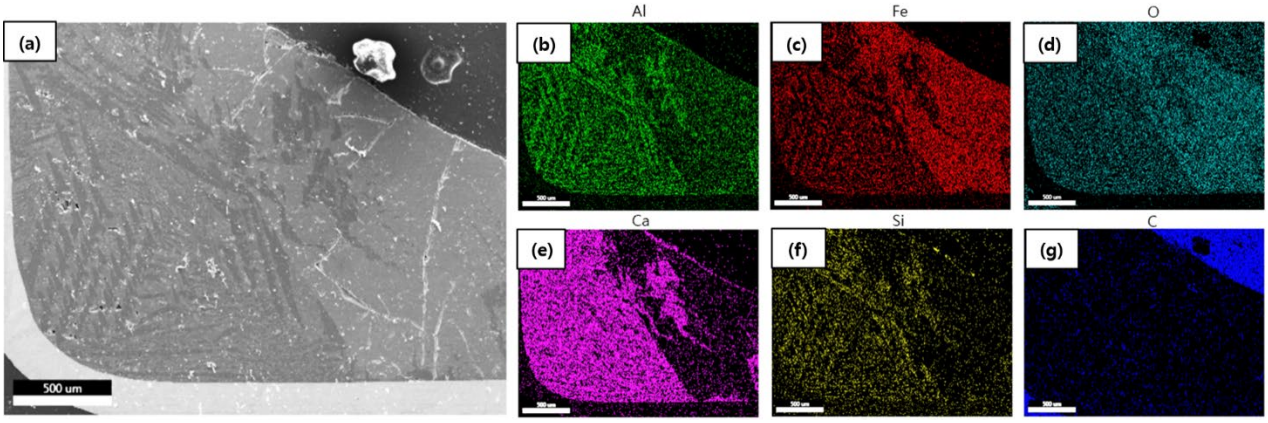

FIG 16 – Locations for EDX analysis for the specimen after the observation of initial surface modification

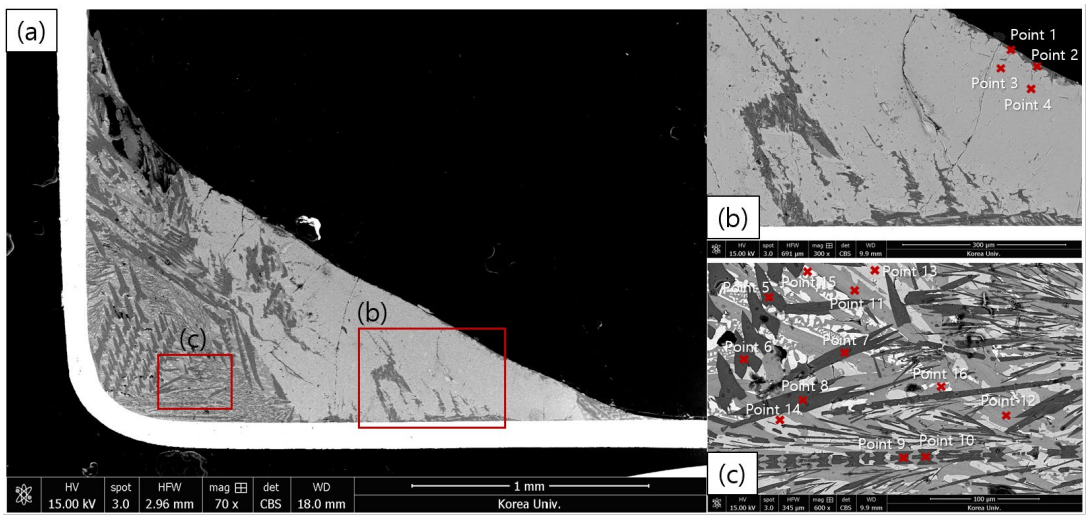

FIG 17 – SEM-BSE analysis of the quenched sample after phase transition-melting melting

TABLE 6 – EDX results of point analysis of FIG 17.

	Elemental Compositions (Atomic Conc, %)						Calculated Compositions (Mole Conc, %)			
	Fe	Ca	Si	Al	O	C	Fe_2O_3	CaO	SiO_2	Al_2O_3
Point 1 (Dark grey)	4.56	14.69	4.08	16.95	52.54	7.18	7.72	49.75	13.82	28.7
Point 2 (Dark grey)	8.28	12.27	4.29	14.54	50.69	9.94	14.8	43.87	15.34	25.99
Point 3 (Light grey)	28.37	0.52	-	9.6	50.08	11.43	72.72	2.67	-	24.61
Point 4 (Light grey)	28.04	0.49	-	9.21	49.26	13	73.35	2.56	-	24.09
Point 5 (Dark grey)	3.29	14.8	4.98	16.67	52.83	7.42	5.53	49.73	16.73	28.01
Point 6 (Dark grey)	3.04	14.9	5.2	16.5	52.3	8.06	5.09	49.88	17.41	27.62
Point 7 (Dark grey)	2.95	14.74	5.36	16.21	51.84	8.9	4.97	49.66	18.06	27.31
Point 8 (Dark grey)	3	14.82	5.04	16.53	53.03	7.58	5.06	50.03	17.01	27.9
Point 9 (Dark grey)	3.28	14.98	4.92	16.72	52.94	7.15	5.48	50.1	16.45	27.96
Point 10 (Dark grey)	3.47	14.94	4.9	16.69	52.95	7.04	5.8	49.93	16.38	27.89
Point 11 (Medium grey)	13.51	20.58	0.68	6.26	51.14	7.82	21.69	66.08	2.18	10.05
Point 12 (Medium grey)	11.91	20.48	0.59	8.16	51.45	7.41	19.14	65.84	1.90	13.12
Point 13 (Medium-light grey)	31.04	0.94	-	6.39	50.94	10.69	78.96	4.78	-	16.26
Point 14 (Medium-light grey)	30.98	0.98	-	6.17	50.66	11.21	79.21	5.01	-	15.78
Point 15 (Light grey)	38.49	1.68	-	1.15	47.12	11.56	89.51	7.81	-	2.67
Point 16 (Light grey)	38.06	1.57	-	1.05	47.45	11.87	90.08	7.43	-	2.49

CONCLUSIONS

The phase transition of SFCA was investigated with DSC and CLSM. The in-situ observation with CLSM was focused on the peak positions observed with DSC. It was found that the peak position was related to the liquid phase formation: initial melting, massive liquid phase formation, and phase transition-melting. The quenched sample revealed that the Fe_3O_4 solid solution appeared as a result of the phase transition of CF and CFA. The results of the present observation can be utilized in designing a new iron ore sinter, which can be used in a hydrogen-enriched ironmaking process.

ACKNOWLEDGEMENTS

This work was supported by the Industrial Strategic Technology Development Program (RS-2023-00262421, Development of basic design technology for hydrogen based ironmaking) funded by the Ministry of Trade, Industry & Energy in the Republic of Korea. This work was also supported by the Korea Institute for Advancement of Technology(KIAT) grant funded by the Government of the Republic of Korea(MOTIE, P0023676, HRD Program for Industrial Innovation)

REFERENCES

Geleta, D, D, and Lee, J, 2018. Effects of Particle Diameter and Coke Layer Thickness on Solid Flow and Stress Distribution in BF by 3D Discrete Element Method, Metallurgical and Materials Transactions B-process Metallurgy and Materials Processing Science, vol. 49, pp 3594-3602

Hamilton, J, G, Hoskins, B, Mumme, W, Borbidge, W, and Montague, M, 1989. The crystal structure and crystal chemistry of Ca2. 3Mg0. 8Al1. 5Si1. 1Fe8. 3O20 (SFCA): solid solution limits and selected phase relationships of SFCA in the SiO2-FeO3-CaO (-Al2O3) system, Neues Jahrbuch für Mineralogie. Abhandlungen, vol. 161, pp 1-26

Murao, R, Harano, T, Kimura, M, Jung, I-H, 2018. Thermodynamic modeling of the SFCA phase Ca2 (Fe, Ca) 6 (Fe, Al, Si) 6O20, ISIJ International, vol.58, pp 259-266

Park, J, Kim, E, Suh, I-K, and Lee, J, 2022. A Short Review of the Effect of Iron Ore Selection on Mineral Phases of Iron Ore Sinter, Minerals, vol.12, 35

Park, J, Kim, E, Suh, I-K, and Lee, J, 2023. Effects of basicity and Al2O3 content on the crystal structure of silico-ferrite of calcium and aluminum, ISIJ International, vol. 63, pp 235-243

Park, J, Ramaraghavulu, R, Suh, I-K, Jeon, J, Son, S, and Lee, J, 2020. Effects of Basicity and Al_2O_3 Content on the Chemistry of Phases in Iron Ore Sinter Containing ZnO, Metallurgical and Materials Transactions B-process Metallurgy and Materials Processing Science, 2020, vol. 51, pp 3016–302

Takayama, T, Murao, R, and Kimura, M, 2018. Quantitative Analysis of Mineral Phases in Iron-ore Sinter by the Rietveld Method of X-ray Diffraction Patterns, ISIJ International, vol. 58, pp 1069-1078

Webster, N, A, S, Pownceby, M, I, Madsen, I, C, Kimpton, J, A, 2012. Silico-ferrite of Calcium and Aluminum (SFCA) Iron Ore Sinter Bonding Phases: New Insights into Their Formation During Heating and Cooling, Metallurgical and Materials Transactions B-process Metallurgy and Materials Processing Science, vol. 43, pp 1344-1357

Webster, N, A, S, Pownceby, M, I, Madsen, I, C, Kimpton, J, A, 2021. Silico-ferrite of Calcium and Aluminum (SFCA) and SFCA-Ⅰ Iron Ore Sinter Bonding Phase Formation: Effects of MgO on Phase Formation During Heating, JOM, vol. 73, pp 299-30

Webster, N, A, S, Pownceby, M, I, Fan, R, and Brand, H, E, A, 2022. Fundamentals of Silico-Ferrite of Calcium and Aluminium (SFCA) and SFCA-I Iron Ore Sinter Bonding Phase Formation: Effects of MgO Source on Phase Formation during Heating, ISIJ International, vol. 62, pp 652-657